www.czasopisma.pan.pl PAN POLSKA AKADEMIA NAUK www.journals.pan.pl

Arch. Metall. Mater. **67** (2022), 1, 303-309

DOI: https://doi.org/10.24425/amm.2022.137756

P. KOPROWSKI[1*], M. LECH-GREGA[1], Ł. WODZINSKI[2], B. AUGUSTYN[1], S. BOCZKAL[1], P. ULIASZ[2], M. OŻÓG[2]

THE EFFECT OF 0.2% ADDITION OF Mg, Co AND Ce ON MICROSTRUCTURE AND MECHANICAL PROPERTIES OF 1XXX SERIES ALUMINIUM ALLOY CASTINGS DESIGNED FOR OVERHEAD TRANSMISSION LINES

The effect of 0.2% addition of Mg, Co and Ce to 99.9% cast aluminium was studied by evaluation of changes in microstructure and mechanical properties. The microstructure was analyzed by scanning electron microscopy and transmission electron microscopy. The Al99.9 alloy contained only Al-Fe-Si phase particles. Similar Al-Fe-Si particles were observed in alloy with 0.2% Mg addition, because this amount of magnesium was fully dissolved in the solid solution. The addition of cobalt resulted in the formation of $Al_{9.02}Co_{1.51}Fe_{0.47}$ phase particles assuming the shape of eutectic plates. The electron backscattered diffraction map made for the alloy with 0.2% Co addition showed numerous twin boundaries with distances between them in the range from 10 to 100 μm. The addition of cerium was located in the grain boundary area. Cerium also gave rise to the formation of two types of particles, i.e. Al_4Ce and Al-Ce-Fe-Si. The Al-Ce-Fe-Si phase is a nucleation site for the Al_4Ce phase, which forms eutectic plates. The results showed that the introduction of additives increases the mechanical properties of the cast materials. The 99.9% cast aluminium has a hardness of 16.9 HB. The addition of 0.2% by weight of Mg, Co, Ce increases this hardness to 21.8 HB, 22.6 HB and 19.1 HB, respectively.

Keywords: Micro-additions; aluminium; hardness; microstructure; overhead transmission lines

1. Introduction

Micro-additions of alloying elements may have positive impact on mechanical properties, grain size and other important parameters of aluminium because of solid solution hardening [1] or formation of fine precipitates that hinder dislocation movement [2]. Micro-additions also have positive impact on clustering before precipitate formation and thermal stability of aluminium and its alloys [3]. Therefore, it is important to estimate the effect of Mg, Co or Ce on microstructure and mechanical properties of aluminium, especially in the production of overhead transmission lines.

In the Al-Mg system, a complex intermetallic Al_3Mg_2 compound, also known as β or Samson phase, appears [4,5]. According to the phase diagram, the presence of other phases, i.e. Al_8Mg_5 and $Al_{3.26}Mg_2$, is also possible [6,7]. The aforementioned phases occur with the addition of Mg above a few weight percent, below this value the Mg atoms remain in the solid solution. The increasing content of atoms in the solid solution causes an intense reduction in conductivity [8]. The Al-Co phase equilibrium system shows that Al_9Co_2 appears as a eutectic [9,10]. This phase crystallizes in a monoclinic structure and has a favourable effect on mechanical properties [11]. Interesting and little-explored additive is cerium - one of the rare earth elements. Literature data suggests the occurrence of two possible types of precipitates, i.e. orthorhombic $Al_{11}Ce_3$ and tetragonal Al_4Ce, but Al_4Ce seems to be a high-temperature phase which does not occur at room temperature [12,13]. Cerium can be an important additive to aluminium alloys, providing the deoxidizing and dehydrogenizing effect and reacting with impurities, thus leading to purification of the solid solution [14]. The particles of other phases also act as scattering centres, and therefore they negatively affect the electrical conductivity by lowering it. However, in the case when the addition of an element causes the formation of particles taking away atoms dissolved in the solid solution, the combined effect may be positive for conductivity [8,15,16].

The purpose of this research was to investigate the microstructure and mechanical properties of three alloys with micro-additions of Mg, Co or Ce. Hardness tests were performed to

[1] ŁUKASIEWICZ RESEARCH NETWORK – INSTITUTE OF NON-FERROUS METALS, DIVISION IN SKAWINA, 19 PIŁSUDSKIEGO STR., 32-050 SKAWINA, POLAND
[2] BORYSZEW S.A., MODERN ALUMINIUM PRODUCTS, 23 PIŁSUDSKIEGO STR., 32-050 SKAWINA, POLAND

* Corresponding author: pkoprowski@imn.skawina.pl

evaluate the effect of each additive on mechanical properties. The microstructure was examined using scanning electron microscope (SEM) equipped with energy dispersive spectroscopy (EDS) detector. The electron backscattered diffraction (EBSD) technique was implemented to obtain crystallographic information. Finally, transmission electron microscopy (TEM) observations were performed.

2. Materials and methods

Four ingots of 100 mm diameter were cast by vertical direct casting method. Al99.9% was used as a base material to which one element was added to obtain the required chemical composition. The chemical composition of ingots was measured by a Baird DV6 optical emission spectrometer and it is shown in Table 1. For each ingot, 30 hardness indentations were made on a radius of 35 mm. Hardness was measured using a Duramin 2500E device operating under a load of 153 N and equipped with a 2.5 mm diameter Brinell indenter. Samples for SEM study were cut out from 3/4 of the ingot radius and prepared by grinding with sandpapers and polishing with diamond suspensions. A Leica EM RES 101 ion-beam polisher was used in the final step of preparation to obtain a perfectly flat surface. A FEI Inspect F50 scanning electron microscope was used for imaging, and EBSD and EDS investigations. Samples were examined on a transverse cross-section. The samples for TEM studies were prepared on a twin-jet electropolisher using a solution of nitric acid and methanol (1:2 ratio) at –22°C. A Tecnai G2 20 transmission electron microscope was used for the microstructural observations and analysis.

TABLE 1

Chemical composition of investigated materials

Designation	Weight percentage [%]						
	Si	Fe	Mg	Ni	Co	Ce	Al
01 – base material	0.040	0.031	0.001	0.001	—	—	balance
02 – Mg addition	0.027	0.035	**0.205**	0.002	—	—	balance
03 – Co addition	0.042	0.063	0.001	0.008	**0.203**	—	balance
04 – Ce addition	0.044	0.050	0.009	0.007	—	**0.195**	balance

3. Results and discussion

The hardness obtained for ingots is shown in Figure 1. The base material had a hardness of about 17 HB. Each additive caused an increase in hardness. The least effective turned out to be cerium with only a 2 HB increase observed. The change was more significant when Mg and Co were added to the alloy. The increase in hardness was 4.9 HB and 5.7 HB for materials 02 and 03, respectively.

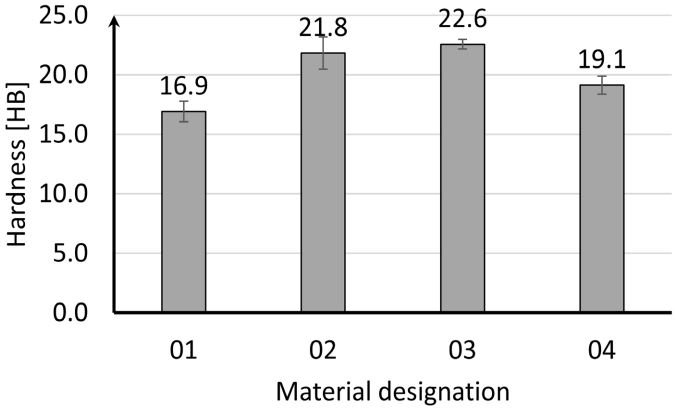

Fig. 1. Hardness of ingots

The microstructure observed at low magnification in all the examined materials is presented in Figure 2. Materials 01 and 02 are nearly free from particles. Only a small number of round and evenly distributed particles is visible (Fig. 2a,b). For both materials, the size of the second phase particles is approximately 1-3 µm. Particles in sample 03 formed a visible network of eutectic mixture around regular α-Al cells (Fig. 2c). Similar microstructure was obtained for Al-0.7 wt% Co alloy castings [17]. The investigated alloys 03 and Al-0.7% Co are hypoeutectic, because according to the literature, the eutectic point occurs at 1.09% by weight of cobalt [9]. The average spacing between cell boundaries is 29.4 µm ± 3.7 µm. Occasionally, in the backscattered electron images, twinned dendrite growth (feathery grains) [18] has been observed as a nearly parallel line of eutectic mixture (marked with yellow line). In previous research, it has been observed that twin boundaries exist in extruded materials and their number even increases after wire drawing process [15]. From that research we have information that twin boundaries were obtained by the formation of twinned dendrites during solidification. The second phase particles with cerium addition are well contrasting and are mainly visible as round or elongated spots (Fig. 2d). Brighter curve is the grain boundary where cerium tends to locate.

The analysis of the chemical composition of particles at higher magnification was performed using EDS detector in SEM. The results obtained for all samples are presented in Figure 3. Each sample contains a small amount of iron and silicon which are impurity elements remaining from the casting process [19]. Fe and Si are mainly part of the particles which were formed during solidification [20]. In the base material (designated as 01), mainly Al-Fe-Si particles were observed. Identical particles were observed in alloy 02. Detailed analysis of materials 01 and 02 suggests that magnesium may also react with silicon, forming the nearly spherical Mg_2Si phase. The main strengthening mechanism for material 02 is solution hardening. The strengthening mechanism is in agreement with the phase equilibrium diagram, where a few percentages of Mg can be dissolved in Al, and also with the research described in literature, where the solution strengthening in Al-Mg alloys is claimed to take place up to a few weight percentages of Mg [21-23].

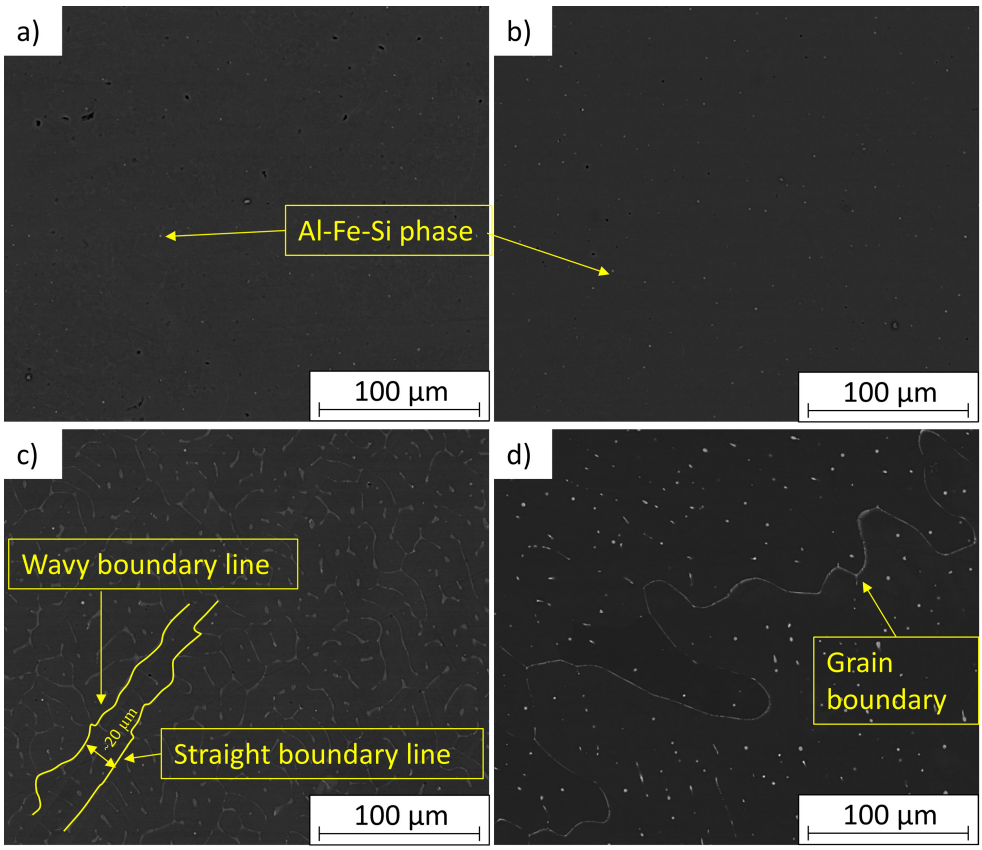

Fig. 2. SEM-BSE images of samples: 01 (a), 02 (b), 03 (c) and 04 (d)

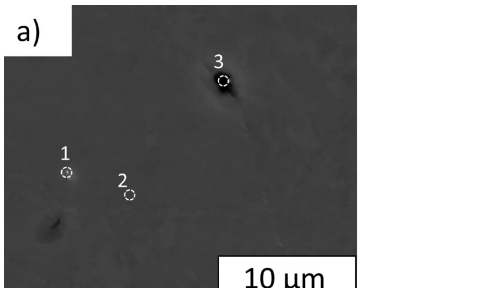

Spot	O [%]	Mg [%]	Al [%]	Si [%]	Fe[%]	Ni [%]
1	-	-	96.7	1.0	1.8	0.5
2	-	-	100.0	-	-	-
3	3.9	2.2	92.5	1.4	-	-

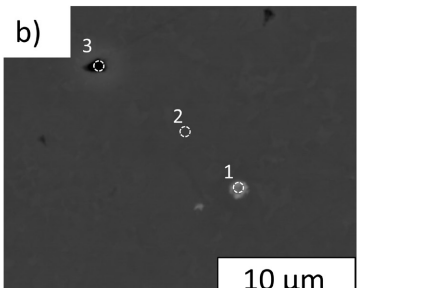

Spot	Al [%]	Fe[%]	Ni [%]	Mg [%]	Si [%]
1	94.6	3.1	0.6	0.2	1.4
2	99.7	-	-	0.3	-
3	97.6	-	-	1.5	0.9

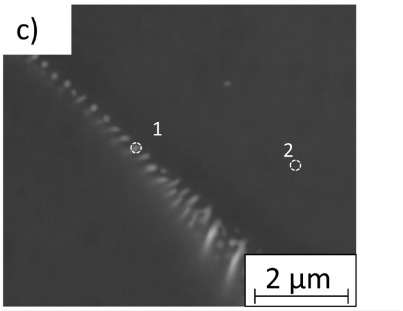

Spot	Al [%]	Fe[%]	Co [%]
1	98.7	0.3	1.0
2	100	-	-

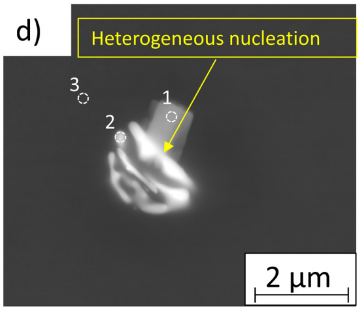

Spot	Al [%]	Si[%]	Fe [%]	Ce [%]
1	95.1	1.6	2.0	1.3
2	97.6	-	-	2.4
3	100	-	-	-

Fig. 3. SEM-BSE images of the particles and EDS results for samples: 01 (a), 02 (b), 03 (c), 04 (d). The results are presented as atomic percentages

The morphology of the second phase particles in alloy 03 is eutectic-like. Particles in the form of plates are alternately located with α-Al phase (Fig. 3c). The length of the plates varies in a wide range of values, i.e. from 200 nm to a few μm. The chemical composition indicates that particles contain Al, Co and Fe atoms. In previous research, these particles were identified as the $Al_{9.02}Co_{1.51}Fe_{0.47}$ phase and the current study confirms this result [15]. Two types of particles are observed in alloy 04 (Fig. 3d). According to the solidification diagram of materials, it is expected that the particle containing Al, Ce, Fe, Si is the first one to form and then this particle becomes a homogenous nucleation site for the Al_4Ce phase. The Al_4Ce phase was detected by the EBSD method and its diffraction pattern is presented in Figure 4. The phase crystallography is tetragonal and it differs significantly from the orthorhombic structure of the $Al_{11}Ce_3$ phase. However, the Al_4Ce phase is a high-temperature phase which should dissolve during casting process. According to the Al-Ce phase diagram, the phase stable at room temperature is the $Al_{11}Ce_3$ phase [12]. It is probable that Fe and Si impurities and high cooling rate during casting process stabilize this phase at room temperature. The literature review shows that various researchers have mentioned the occurrence of the Al_4Ce phase [24,25] and $Al_{11}Ce_3$ phase at room temperature [26,27].

The EBSD maps made for materials 01, 02 and 04 indicate a large grain size which is typical for cast materials. An exception is material 03. For this alloy, the EBSD map has indicated the occurrence of twinned/untwinned areas (Fig. 5). Detailed analysis showed that the boundary plane is related to the (111) plane, and the misorientation angle is close to 60°. Observations demonstrate that twins have a straight and curved/wavy twin boundary line. According to M.A. Salgado-Ordorica and M. Rappaz [18], the straight line is a coherent twin boundary, and the wavy line is an incoherent twin boundary. The point-to-point misorientation profile analysis has shown that all coherent boundaries exhibit a 59.8º misorientation angle, while the misorientation angle of incoherent boundaries varies from 59.1º to 59.7º. The untwinned spacing is typically from 5 to 13 times larger than the twinned one. It is also worth emphasizing that the composition of alloy 03 is significantly diluted in comparison to other materials where twin boundaries were observed [18,28].

The TEM analysis for material 03 has confirmed the presence of $Al_{9.02}Co_{1.51}Fe_{0.47}$ phase particles (Fig. 6). According to the results obtained by Bostrom et al. [29] and Grushko et al. [30], this phase has a crystallographic cell nearly identical to Al_9Co_2 with slightly changed lattice parameters The iron content is responsible for the difference in the lattice type. The particles form eutectic plates. Based on all observations carried out for material 03, it can be concluded that the increase in hardness is caused by the presence of particles that are obstacles to the dislocation movement through Orowan mechanism or dispersion strengthening [31]. A significant number of twin boundaries is another factor strongly influencing the strengthening effect, since these boundaries are also acting as barriers to the dislocation movement [32].

The sample with the addition of cerium (designated as 04) was also analyzed using transmission electron microscopy (Fig. 7). Two types of particles were observed, i.e. Al-Ce-Fe-Si

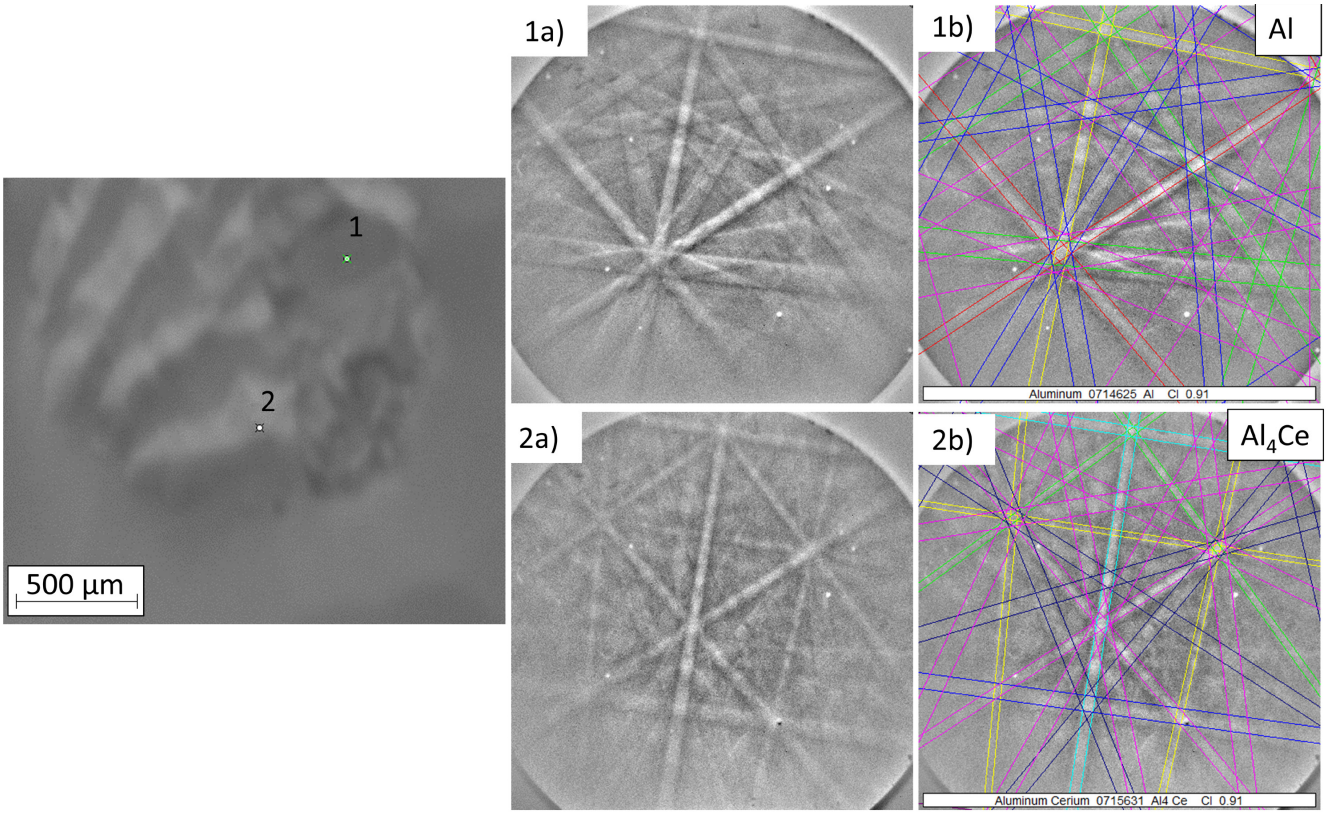

Fig. 4. SEM-SE image of the particles with Kikuchi line analysis in selected places. Sample designated as 04. Raw camera image (1a, 2a), indexed image (1b, 2b). Numbers indicate spot of analysis

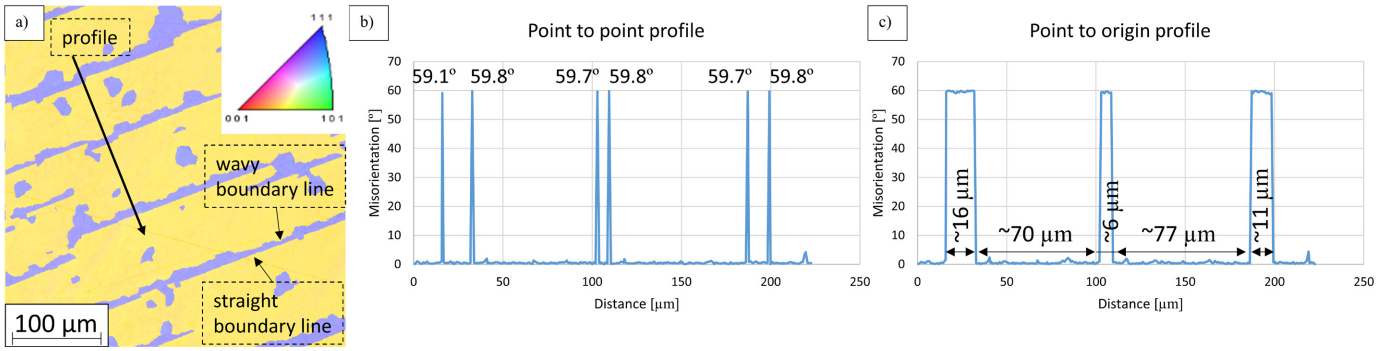

Fig. 5. EBSD map (a) with misorientation point-to-point profile (b) and point-to-origin profile (c) obtained for sample with Co addition

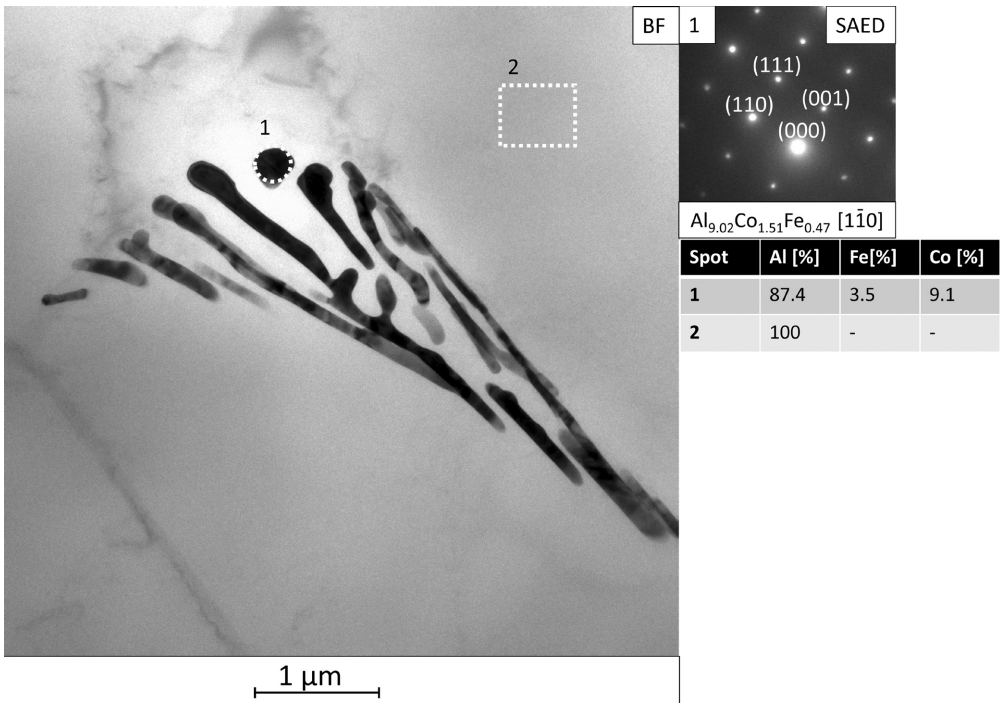

Spot	Al [%]	Fe[%]	Co [%]
1	87.4	3.5	9.1
2	100	-	-

Fig. 6. Bright field image with selected area diffraction pattern and EDS results from $Al_{9.02}Co_{1.51}Fe_{0.47}$ phase. The results are presented as atomic percentages

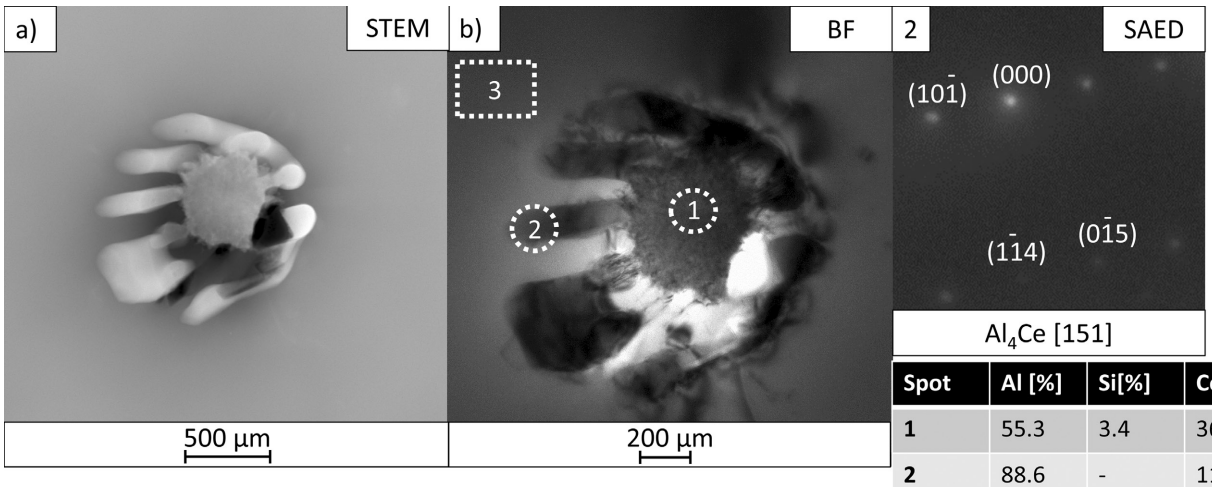

Spot	Al [%]	Si[%]	Ce [%]	Fe [%]
1	55.3	3.4	36.6	4.7
2	88.6	-	11.4	-
3	100	-	-	-

Fig. 7. STEM image (a) and bright field image (b) with selected area diffraction pattern and EDS results of phases in cerium-containing sample. The results are presented as atomic percentages

and Al_4Ce. The Al_4Ce particle was captured during the beginning of nucleation, where its first plates appeared on the Al-Ce-Fe-Si particle. The plates have a width in the range from 150 to 200 nm, while the distances between them vary from a few nm to about 200 nm. In the case of this material, the appearance of particles is mainly identified with the increase in hardness through dispersion strengthening [31].

4. Conclusions

The results allowed drawing the following conclusions:

- Magnesium is the additive that dissolves in aluminum causing solution strengthening. A small part of it is involved in the formation of the Mg_2Si phases,
- The addition of 0.2% cobalt results in the formation of the $Al_{9.02}Co_{1.51}Fe_{0.47}$ phase, which occurs in the form of plates producing a eutectic mixture. Moreover, cobalt causes feathery grain growth observed as twin boundaries in the microstructure. Cobalt increases the strength of the materials through the formation of twin boundaries and Orowan/dispersion strengthening,
- Cerium added to aluminium at a 0.2% content level causes the appearance of two types of particles. The Al-Ce-Fe-Si phase forms first and is acting as a nucleation site for the Al_4Ce phase. The occurrence of the Al_4Ce phase at room temperature is quite unexpected, and therefore extensive studies of this issue should be carried out in the future. Cerium mainly enhances the material strength by dispersion strengthening,
- The addition of Co and Ce reduces the amount of dissolved impurities such as Fe and Si in aluminium solid solution. Properly added, these elements can prove beneficial for materials designed for overhead transmission lines, where atoms retained in the α-Al solid solution generate the undesired scattering of electrons and reduced conductivity.

Acknowledgements

The research was supported by grant of European Funds Smart Growth Operational Programme 2014-2020, project number: POIR.04.01.04-00-0022/15

REFERENCES

[1] J. Kreyca, E. Kozeschnik, State parameter-based constitutive modelling of stress strain curves in Al-Mg solid solutions, International Journal of Plasticity **103**, 67-80 (2018). DOI: https://doi.org/10.1016/J.IJPLAS.2018.01.001

[2] J.D. Embury, D.J. Lloyd, T.R. Ramachandran, Strengthening mechanisms in aluminum alloys, A.K. Vasudevan, R.D. Doherty (Eds.), Aluminum alloys – contemporary research and applications, San Diego, Academic Press, 579-604 (1989).

[3] X. Sauvage, S.S. Lee, K. Matsuda, Z. Horita, Origin of the influence of Cu or Ag micro-additions on the age hardening behavior of ultrafine-grained Al-Mg-Si alloys, Journal of Alloys and Compounds **710**, 199-204 (2017). DOI: https://doi.org/10.1016/j.jallcom.2017.03.250

[4] S. Samson, The Crystal Structure of the phase β-Mg2Al3, Acta Crystallographica **19**, 401-413 (1965). DOI: https://doi.org/10.1107/S0365110X65005133

[5] R. Goswami, G. Spanos, P.S. Pao, R.L. Holtz, Precipitation behaviour of the β phase in Al-5083, Materials Science and Engineering A **527** (4-5), 1089-1095 (2010). DOI: https://doi.org/10.1016/j.msea.2009.10.007

[6] L.F. Mondolfo, Aluminum Alloys: Structure and Properties, London: Butterworths, (1976).

[7] J. Dolinšek, T. Apih, P. Jeglič, I. Smiljanić, A. Bilušić, Z. Bihar, A. Smontara, Z. Jagličić, M. Heggen, M. Feuerbacher, Magnetic and transport properties of the giant-unit-cell Al3.26Mg2 complex metallic alloy, Intermetallics **15** (10), 1367-1376 (2007). DOI: https://doi.org/10.1016/j.intermet.2007.04.010

[8] F. Fickett, A review of resistive mechanisms in aluminium, Cryogenics **11**, 349-367 (1971). DOI: https://doi.org/10.1016/0011-2275(71)90036-1

[9] X. Li, L. Liu, Y. Jiang, G. Huang, X. Wang, Y. Jiang, J. Liang, L. Zhang, X. Shi, Thermodynamic evaluation of the phase equilibria and glass-forming ability of the Al-Co-Gd system, Calphad: Computer Coupling of Phase Diagrams and Thermochemistry **52**, 57-65 (2016). DOI: https://doi.org/10.1016/j.calphad.2015.11.002

[10] E. Stein, C. He, N. Dupin, Melting Behavior and Homogeneity Range of B2 CoAl and Updated Thermodynamic Description of the Al-Co System, Intermetallics **39**, 58-68 (2013). DOI: https://doi.org/10.1016/j.intermet.2013.03.011

[11] B. Grushko, R. Wittenberg, K. Bickmann, C. Freiburg, The constitution of aluminum-cobalt alloys between Al5Co2 and Al9Co2, Journal of Alloys and Compounds **233** (1-2), 279-287 (1996). DOI: https://doi.org/10.1016/0925-8388(95)02045-4

[12] Y. Kang, A.D. Pelton, P. Chartrand, P. Spencer, C.D. Fuerst, Critical Evaluation and Thermodynamic Optimization of the Binary Systems in the Mg-Ce-Mn-Y System, Journal of Phase Equilibria and Diffusion **28**, 342-354 (2007). DOI: https://doi.org/10.1007/s11669-007-9095-9

[13] M.C. Gao, N. Ünlü, G.J. Shiflet, M. Mihalkovic, M. Widom, Reassessment of Al-Ce and Al-Nd binary systems supported by critical experiments and first-principles energy calculations, Metallurgical and Materials Transactions A **36**, 3269-3279 (2005). DOI: https://doi.org/10.1007/s11661-005-0001-y

[14] L. Pengfei, W. Zhigang, W. Yunli, G. Xizhu, W. Zaiyum, L. Zhiqiang, Effect of Cerium on Mechanical Performance and Electrical Conductivity of Aluminum Rod for Electrical Purpose, Journal of Rare Earth **24** (1), 355-357 (2006). DOI: https://doi.org/10.1016/S1002-0721(07)60400-1

[15] P. Koprowski, M. Lech-Grega, Ł. Wodziński, B. Augustyn, S. Boczkal, M. Ożóg, P. Uliasz, J. Żelechowski, W. Szymański, The effect of low content additives on strength, resistivity and microstructural changes in wire drawing of 1xxx series aluminium alloys for

electrical purposes, Materials Today Communications **24**, 101039 (2020). DOI: https://doi.org/10.1016/j.mtcomm.2020.101039

[16] Q. Zhao, Z. Qian, X. Cui, Y. Wu, X. Liu, Influences of Fe, Si and homogenization on electrical conductivity and mechanical properties of dilute Al-Mg-Si alloy, Journal of Alloys and Compounds **666**, 50-57 (2016). DOI: https://doi.org/10.1016/j.jallcom.2016.01.110

[17] C.A.P. Silva, R. Kakitani, M.V. Canté, C. Brito, A. Garcia, J.E. Spinelli, N. Cheung, Microstructure, phase morphology, eutectic coupled zone and hardness of Al-Co alloys, Materials Characterization **169**, 110617 (2020). DOI: https://doi.org/10.1016/j.matchar.2020.110617

[18] M.A. Salgado-Ordorica, M. Rappaz, Twinned dendrite growth in binary aluminum alloys, Acta Materialia **56**, 5708-5718 (2008). DOI: https://doi.org/10.1016/j.actamat.2008.07.046

[19] L. Zhang, J. Gao, L. Nana, W. Damoah, D. Robertson, Removal of iron from aluminium: a review, Mineral Processing and Extractive Metallurgy Review **33**, 99-157 (2012). DOI: https://doi.org/10.1080/08827508.2010.542211

[20] Z.P. Que, Y. Wang, Z. Fan, Formation of the Fe-containing intermetallic compounds during solidification of Al-5Mg-2Si-0.7 Mn-1.1 Fe alloy, Metallurgical and Materials Transactions A **49**, 2173-2181 (2018). DOI: https://doi.org/10.1007/s11661-018-4591-6

[21] E.L. Huskins, B. Cao, K.T. Ramesh, Strengthening mechanisms in an Al-Mg alloy, Materials Science and Engineering: A **527**, 1292-1298 (2010). DOI: https://doi.org/10.1016/j.msea.2009.11.056

[22] R. Kalsar, D. Yadav, A. Sharma, H.-G. Brokmeier, J. May, H.W. Höppel, W. Skrotzki, S. Suwas, Effect of Mg content on microstructure, texture and strength of severely equal channel angular pressed aluminium-magnesium alloys, Materials Science and Engineering: A **797**, 140088 (2020). DOI: https://doi.org/10.1016/j.msea.2020.140088

[23] H. Okamoto, Supplemental Literature Review of Binary Phase Diagrams: Al-Mg, Bi-Sr, Ce-Cu, Co-Nd, Cu-Nd, Dy-Pb, Fe-Nb, Nd-Pb, Pb-Pr, Pb-Tb, Pd-Sb, and Si-W, Journal of Phase Equilibria and Diffusion **36**, 183-195 (2015). DOI: https://doi.org/10.1007/s11669-014-0359-x

[24] H. Cai, F. Guo, X. Ren, J. Su, B. Chen, Effects of cerium on as-cast microstructure of AZ91 magnesium alloy under different solidification rates, Journal of Rare Earths **34** (7), 736-741 (2016). DOI: https://doi.org/10.1016/S1002-0721(16)60085-6

[25] J. Su, F. Guo, H. Cai, L. Liu, Structural analysis of Al-Ce compound phase in AZ-Ce cast magnesium alloy, Journal of Materials Research and Technology **8** (6), 6301-6307 (2019). DOI: https://doi.org/10.1016/j.jmrt.2019.07.042

[26] A. Plotkowski, K. Sisco, S. Bahl, A. Shyam, Y. Yang, L. Allard, P. Nandwana, A.M. Rossy, R. Dehoff, Microstructure and properties of a high temperature Al-Ce-Mn alloy produced by additive manufacturing, Acta Materialia **196**, 595-608 (2020). DOI: https://doi.org/10.1016/j.actamat.2020.07.014

[27] Y. Sun, C. Hung, R.J. Hebert, C. Fennessy, S. Tulyani, M. Aindow, Eutectic microstructures in dilute Al-Ce and Al-Co alloys, Materials Characterization **154**, 269-276 (2019). DOI: https://doi.org/10.1016/j.matchar.2019.06.010

[28] L. Yang, S. Li, K. Fan, Y. Li, Y. Chen, W. Li, D. Kong, P. Cao, H. Long, A. Li, Twin crystal structured Al-10 wt.% Mg alloy over broad velocity conditions achieved by high thermal gradient directional solidification, Journal of Material Science & Technology **71**, 152-162 (2021). DOI: https://doi.org/10.1016/j.jmst.2020.07.032

[29] M. Bostrom, H. Rosner, Y. Prots, U. Burkhardt, Y. Grin, The Co2Al9 Structure Type Revisited, Zeitschrift für anorganische und allgemeine Chemie **631**, 534-541 (2005). DOI: https://doi.org/10.1002/zaac.200400418

[30] B. Grushko, W. Kowalski, M. Surowiec, On the constitution of the Al-Co-Fe alloy system, Journal of Alloys and Compounds **491**, L5-L7 (2010). DOI: https://doi.org/10.1016/j.jallcom.2019.152110

[31] B.A. Szajewski, J.C. Crone, J. Knap, Analytic model for the Orowan dislocation-precipitate bypass mechanism, Materialia **11**, 100671 (2020). DOI: https://doi.org/10.1016/j.mtla.2020.100671

[32] L. Liu, J. Chen, T. Fan, S. Shang, Q. Shao, D. Yuan, Y. Dai, The stability of deformation twins in aluminum enhanced by alloying elements, Journal of Materials Science & Technology **35** (11), 2625-2629 (2019). DOI: https://doi.org/10.1016/j.jmst.2019.07.029